Electronic Supplementary Information

FeP@Foam-Like Graphenic Scaffolds Multi-Yolks/Shell Structure: Strong P-C Bonds and Electrolyte- and Binder- Optimizing Boost Potassium Storage

Qiwei Tan,‡[a] Wang Zhao,‡[a] Kun Han,[a] Ping Li,*[a] Wei (Alex) Wang,*[b] Donglin He,[a] Zhiwei Liu,[a] Qiyao Yu,[c] Mingli Qin[a] and Xuanhui Qu[a]

[a] *Beijing Advanced Innovation Center for Materials Genome Engineering, Institute for Advanced Materials and Technology, University of Science and Technology Beijing, Beijing 100083, China.*

Email: ustbliping@126.com

[b] *John A. Paulson School of Engineering and Applied Sciences, Harvard University, Cambridge, MA 02138, USA.*

Email: wwang3@g.harvard.edu

[c] *Institute of Advanced Structure Technology, Beijing Institute of Technology, Beijing 100081, China*

‡ These authors contributed equally to this work.

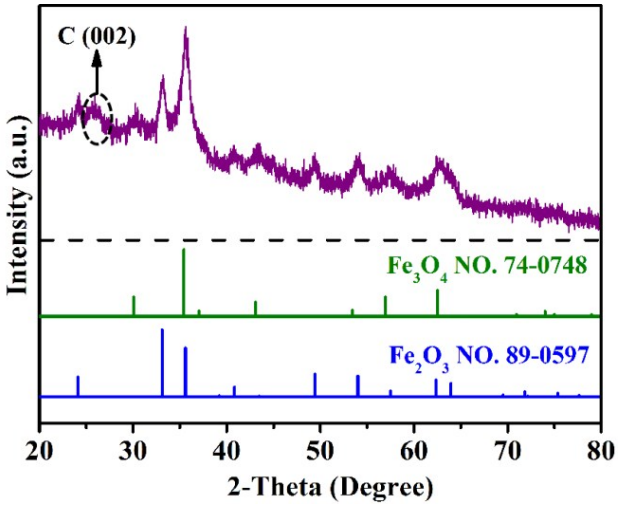

Fig. S1 (a) XRD pattern of the Fe_xO@FGCS precursor.

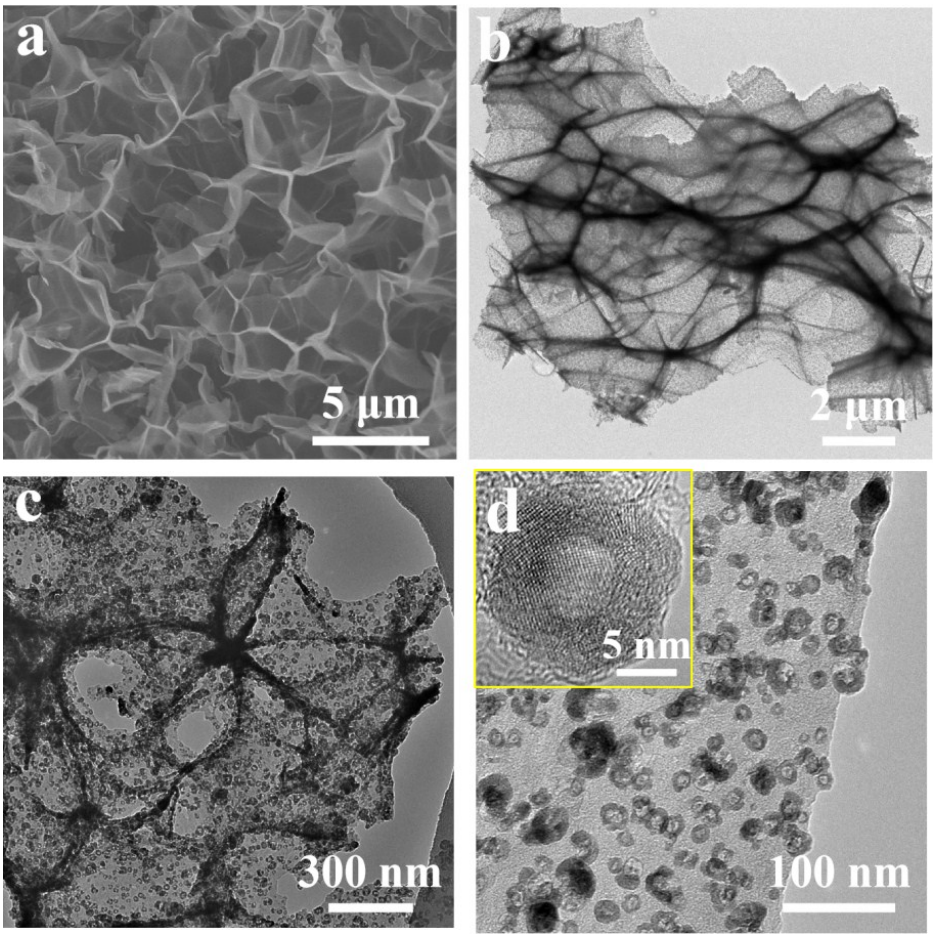

Fig. S2 (a) FESEM micrographs and (b-d) TEM micrographs of the Fe_xO@FGCS precursor.

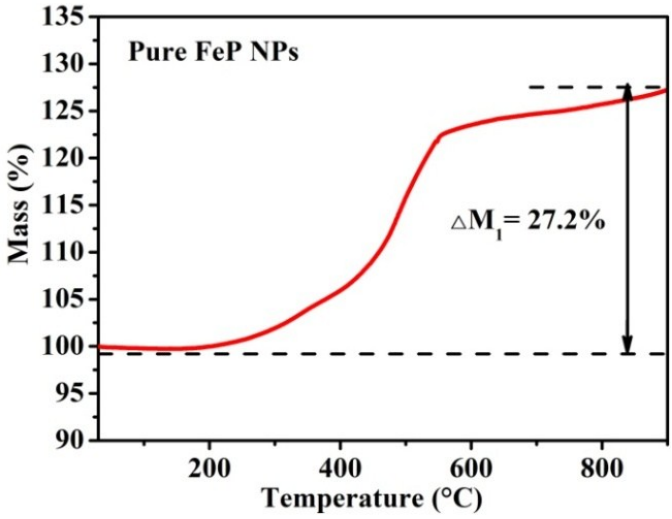

Fig. S3 TGA curve of the pure FeP NPs measured in air atmosphere.

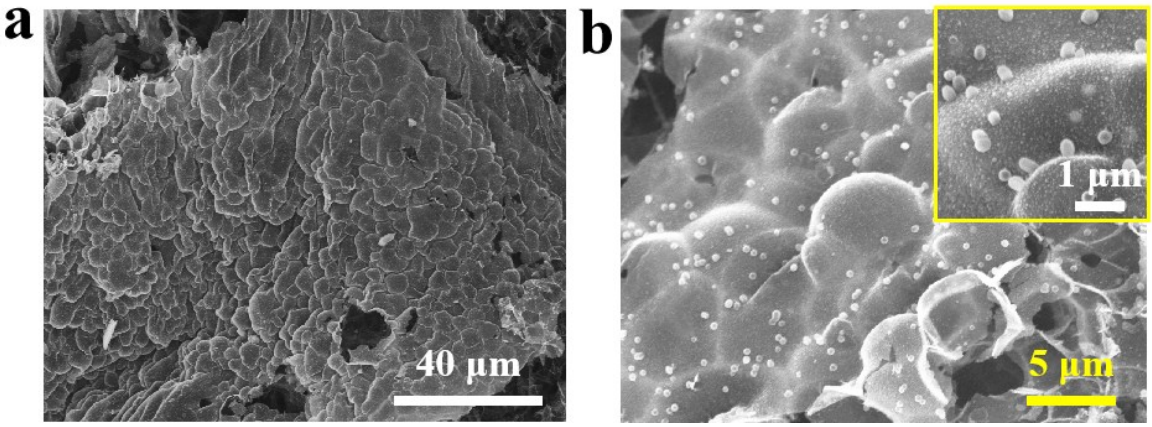

Fig. S4 (a) Low magnification and (b) High magnification FESEM images of the exterior surface of the FeP@FGCS scaffold with uniformly incorporated FeP NPs.

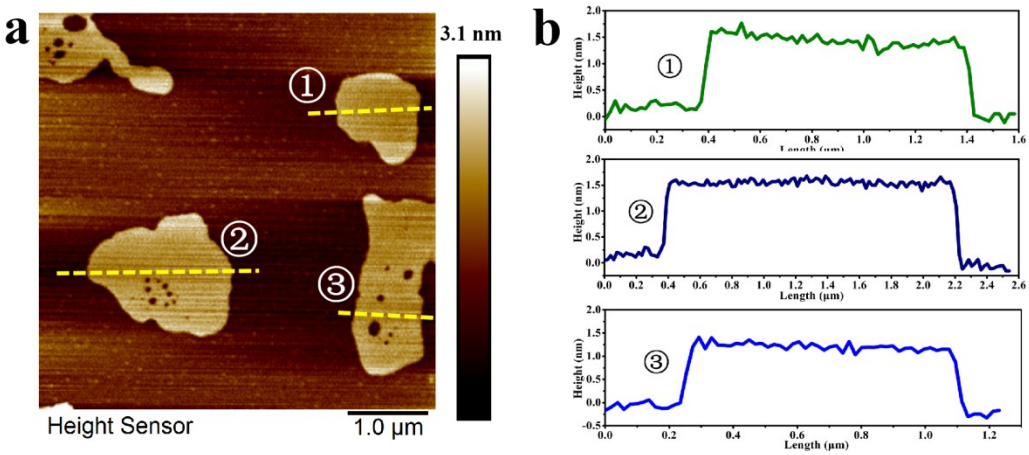

Fig. S5 (a) AFM image of multiple randomly selected nanosheets of the FeP@FGCS with (b) Corresponding height distribution profiles.

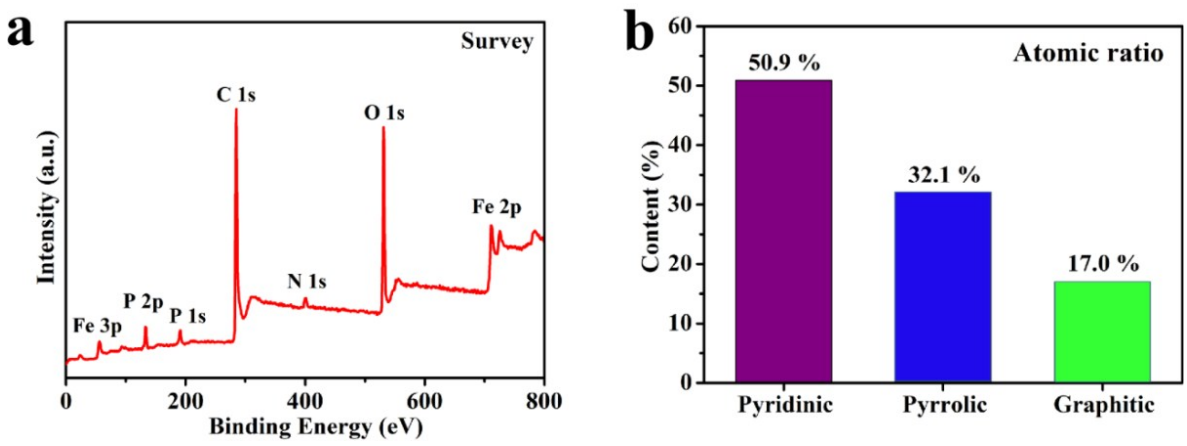

Fig. S6 (a) XPS full survey profile of the FeP@FGCS, (b) calculated atomic ratios of three species of doped N atoms in the FeP@FGCS composite from fitted result in high-resolutional N 1s spectrum.

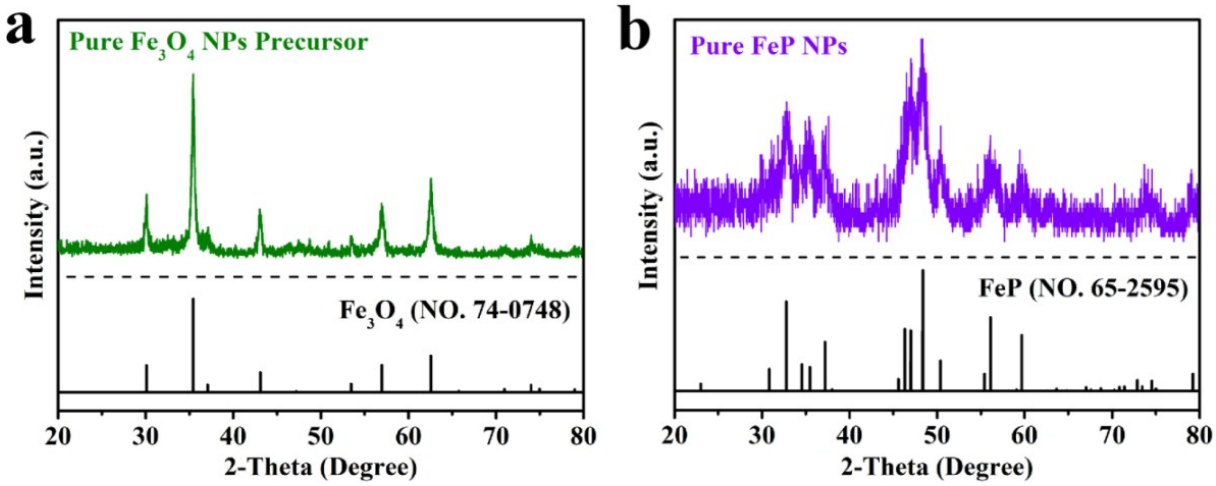

Fig. S7 XRD patterns of (a) the pure Fe_3O_4 NPs precursor synthesized *via* solvothermal method and (b) the obtained pure FeP NPs after the phosphorization treatment.

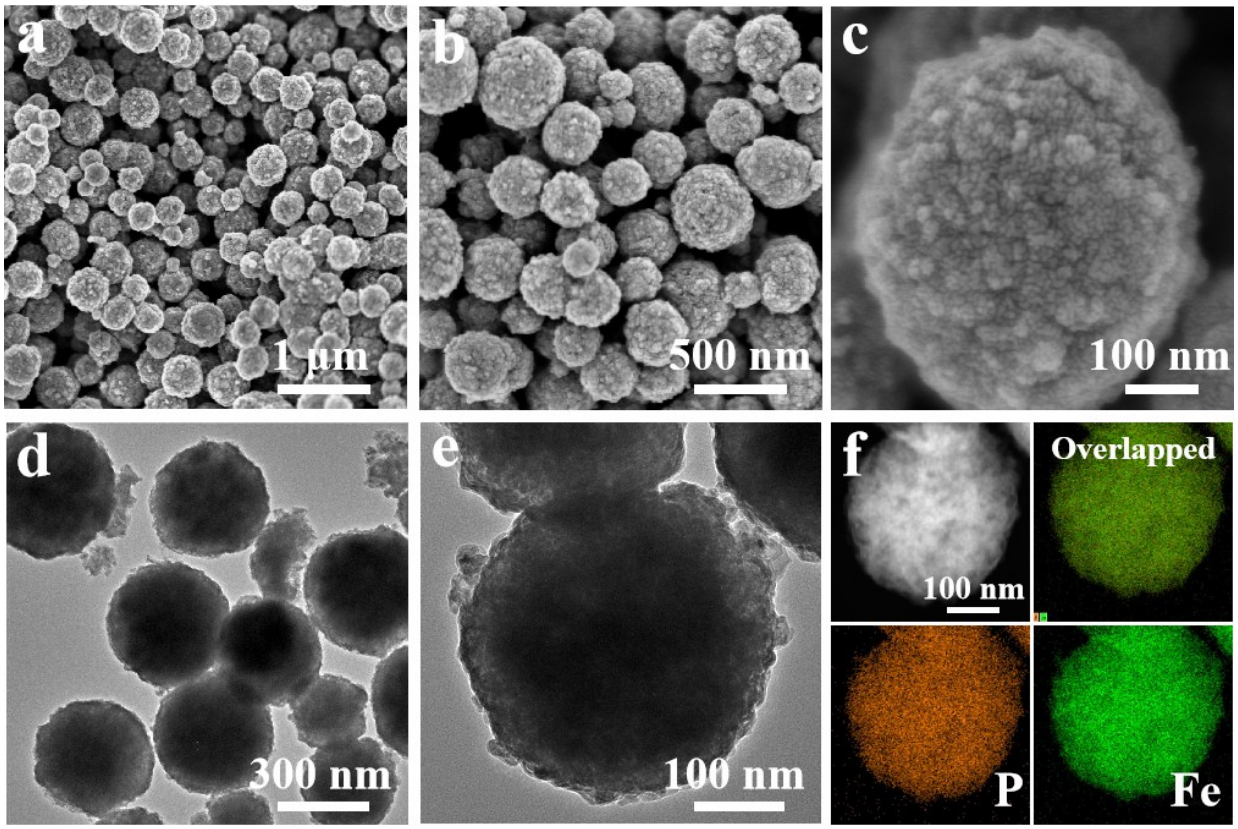

Fig. S8 (a-c) FESEM micrographs of the obtained pure FeP NPs. (d-e) TEM micrographs and (f) corresponding elemental mappings of the obtained pure FeP NPs.

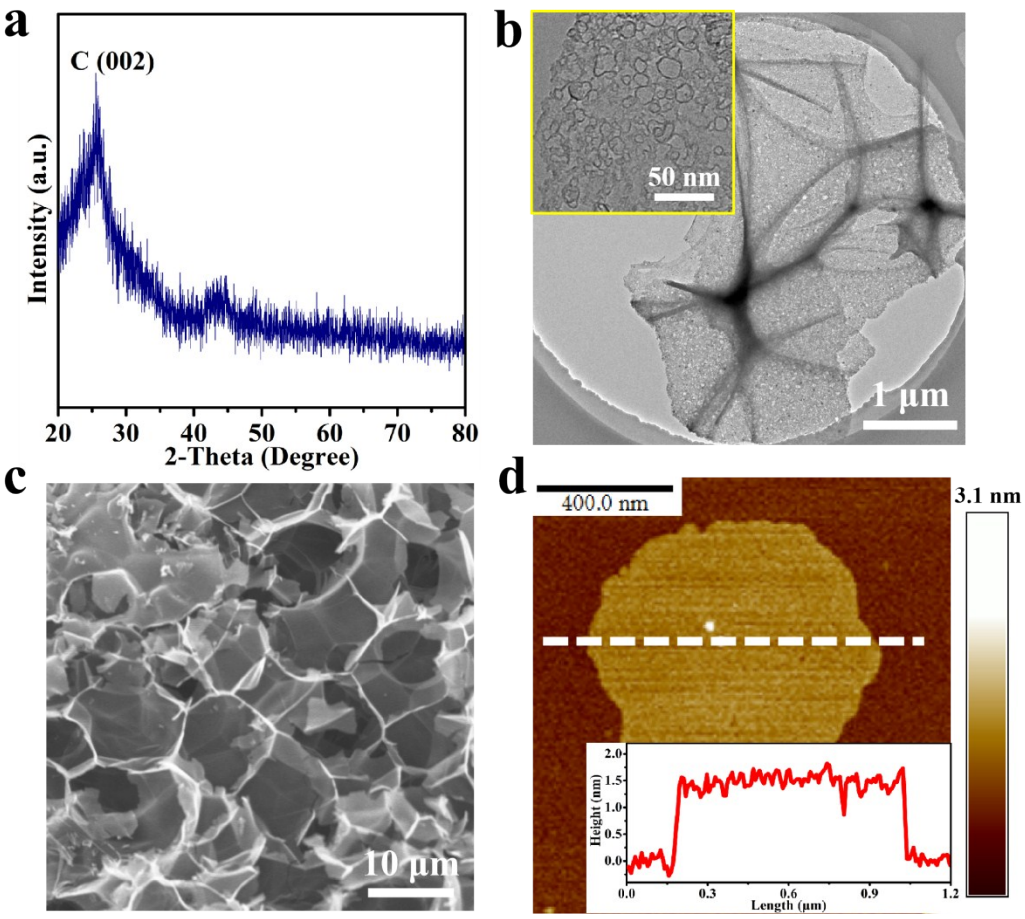

Fig. S9 (a) XRD, (b) Low magnification and high magnification TEM (inset) images of the v-FGCS. (c) FESEM and (d) AFM images with corresponding height distribution profile (inset) of the v-FGCS nanosheet.

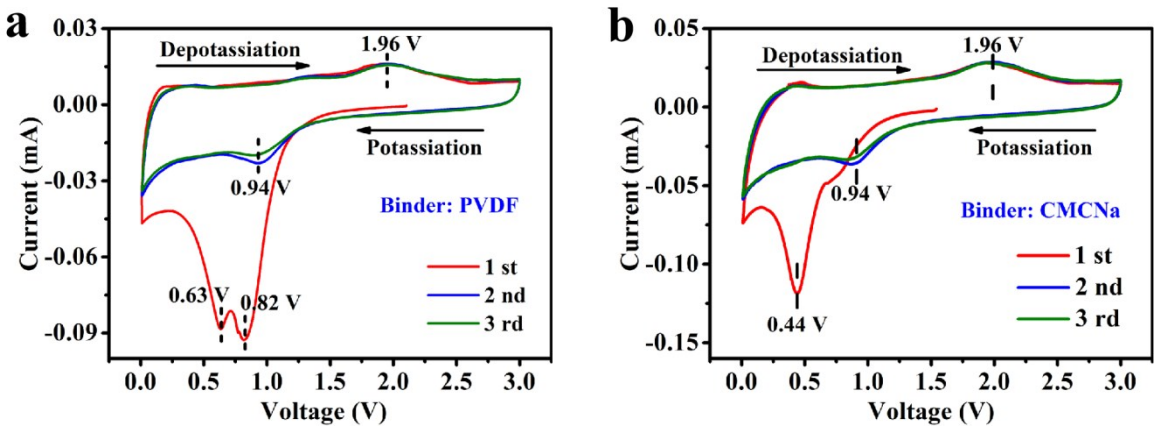

Fig. S10 Cyclic voltammetry curves of the FeP@FGCS electrodes respectively prepared using (a) PVDF and (b) CMCNa as the binder at a sweep rate of 0.1 mV s^{-1}.

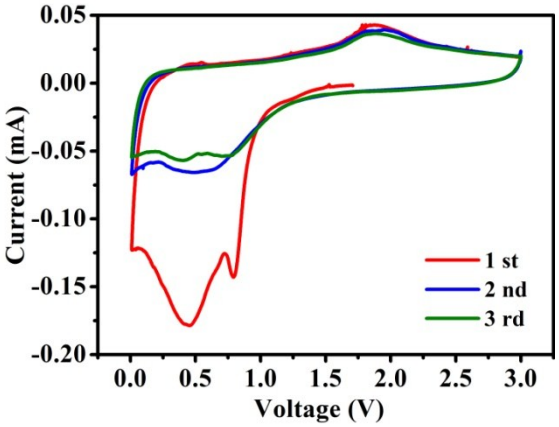

Fig. S11 (a) Cyclic voltammetry curves of the pure FeP NPs measured at a sweep rate of 0.1 mV s^{-1}.

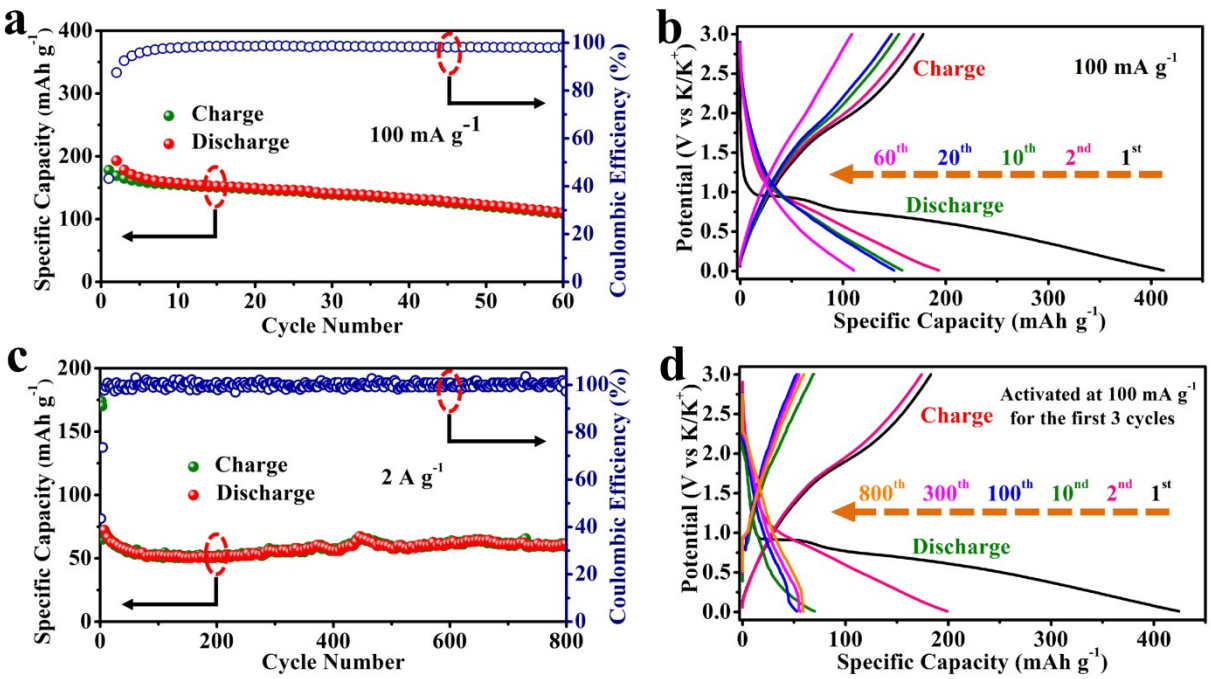

Fig. S12 (a) Cycling performance and (b) the corresponding potential versus specific capacity curves of pure FeP NPs at 100 mA g^{-1} over 60 cycles. (c) Cycling performance and (d) the corresponding potential versus specific capacity curves of pure FeP NPs at 2 A g^{-1} over 800 cycles.

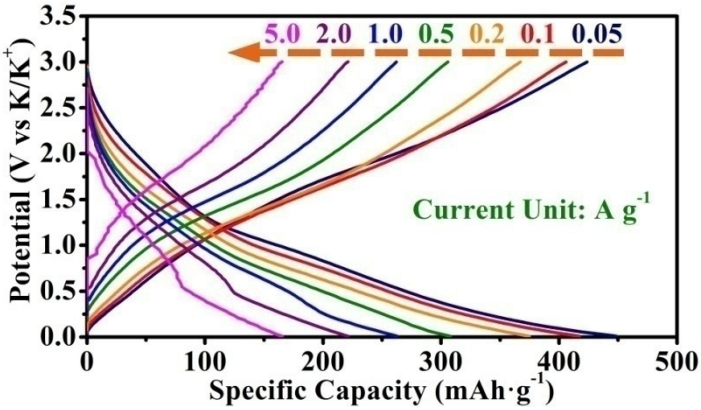

Fig. S13 Potential versus specific capacity curves of the FeP@FGCS at various current densities from 0.05 to 5 A g^{-1}.

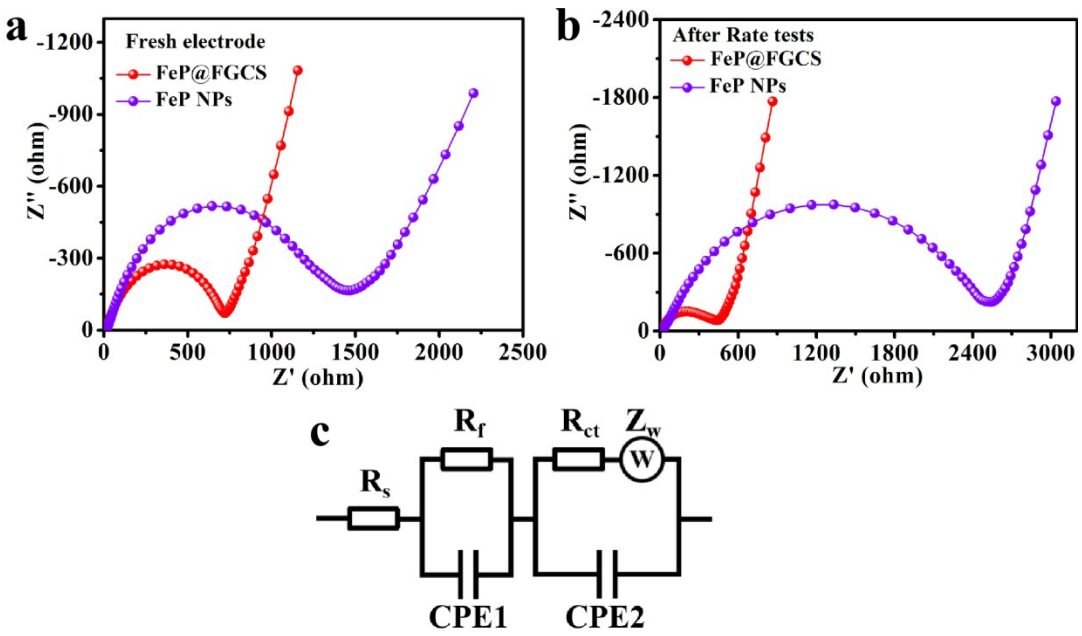

Fig. S14 Nyquist profiles of the FeP@FGCS and pure FeP NPs electrodes (a) before and (b) after rate tests. (c) Equivalent model used for fitting the experimental data.

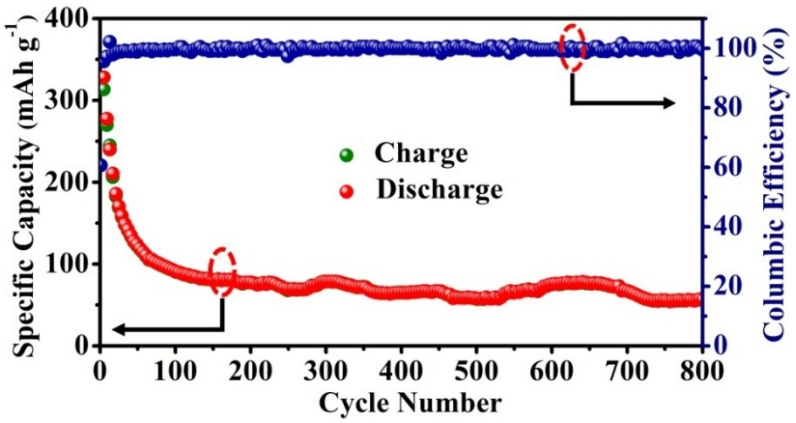

Fig. S15 Cycling performance of the v-FGCS electrode measured at 2 A g^{-1} for 800 cycles.

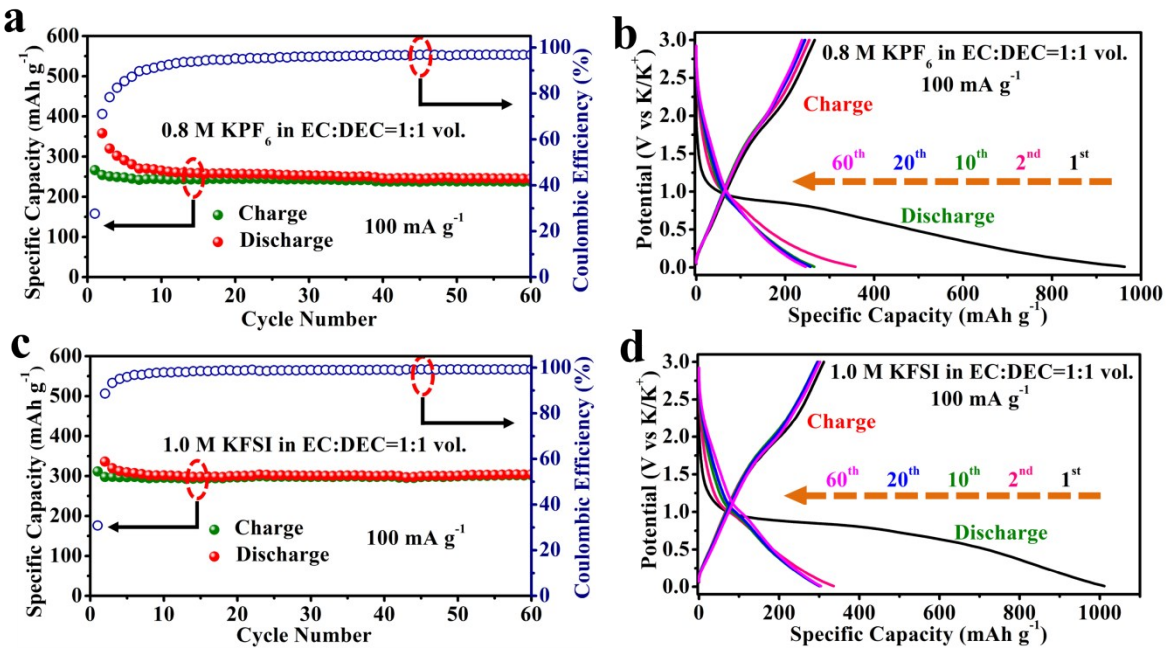

Fig. S16 (a) Charge-discharge profiles and (b) the corresponding potential versus specific capacity curves of the FeP@FGCS electrode using 0.8 M KPF_6 in EC:DEC (1:1 vol.) at 100 mA g^{-1}. (c) Charge-discharge profiles and (d) the corresponding potential versus specific capacity curves of the FeP@FGCS electrode using 1.0 M KFSI in EC:DEC (1:1 vol.) at 100 mA g^{-1}.

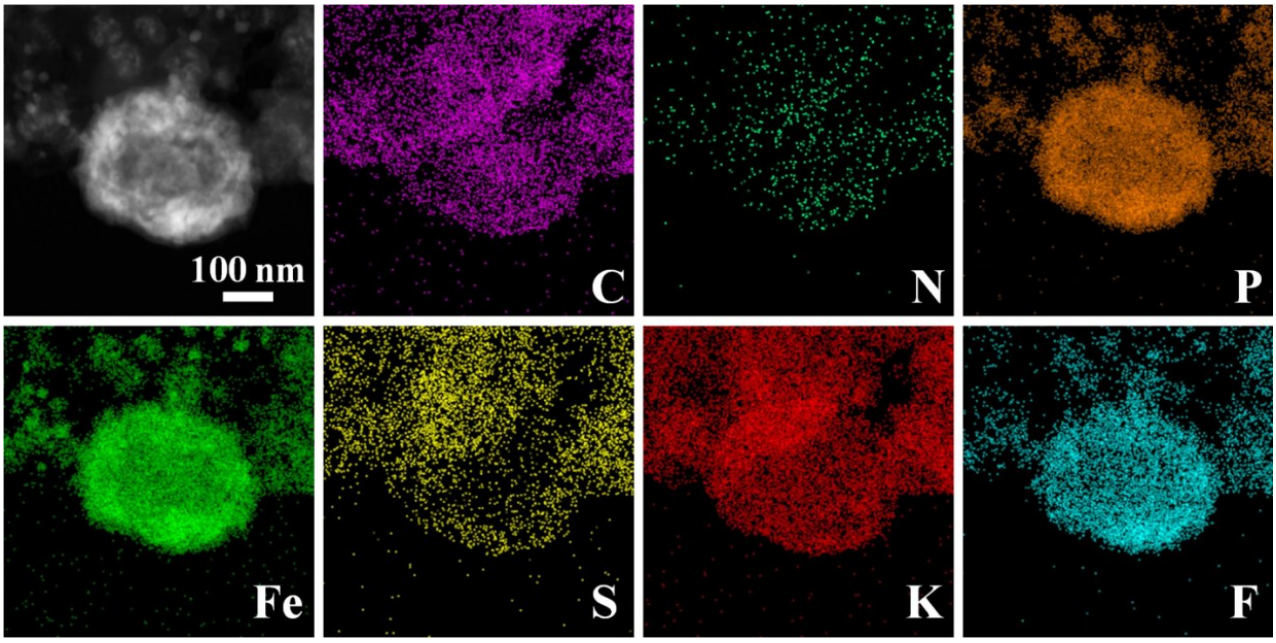

Fig. S17 HAADF-STEM micrograph and the corresponding elemental mappings of the FeP@FGCS electrode using 1.0 M KFSI in DME as electrolyte after 200 cycles at 2 A g^{-1}.

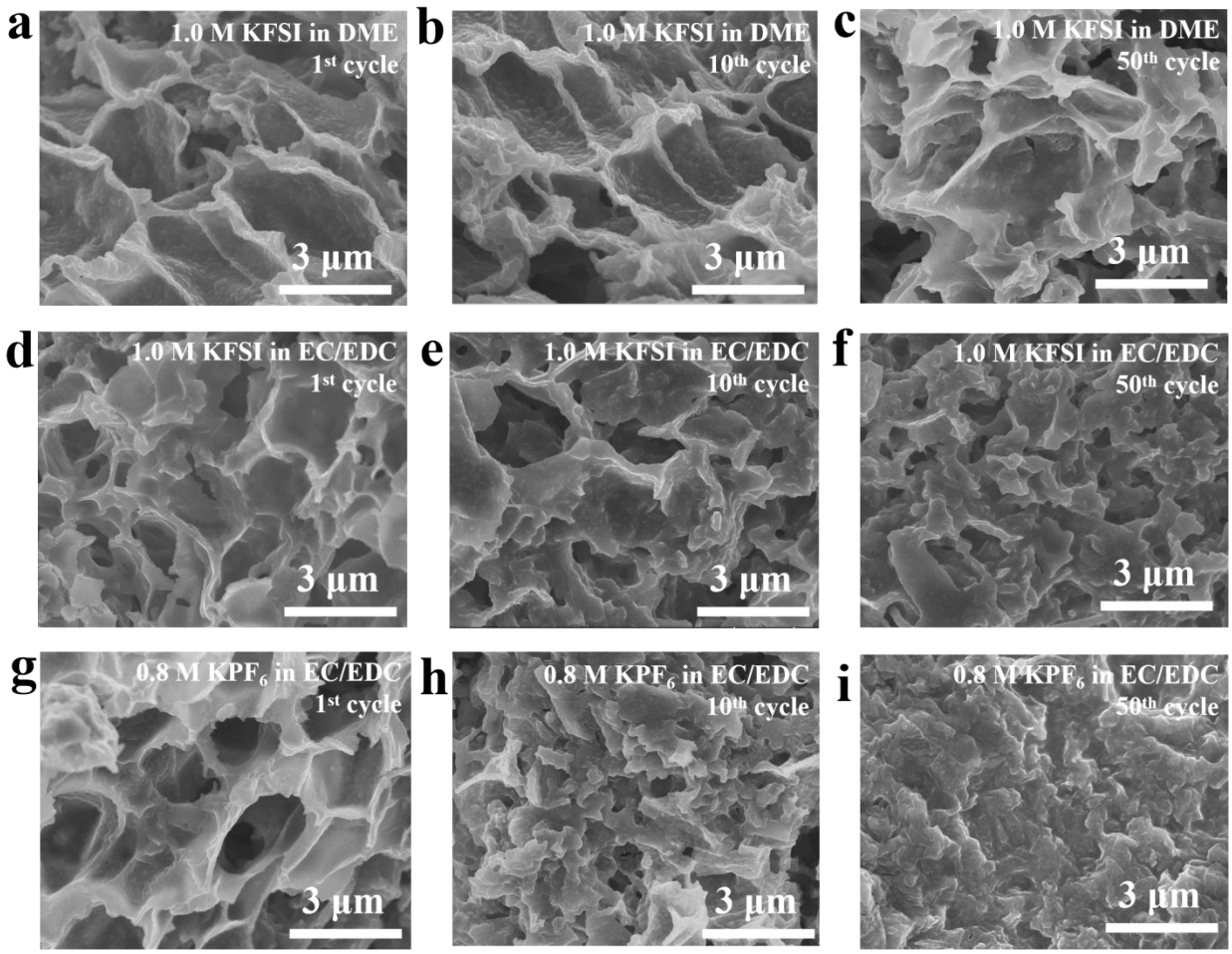

Fig. S18 FESEM images of the FeP@FGCS electrodes (a-c) after 1, 10 and 50 cycles in 1.0 M KFSI in DME electrolyte. (d-e) After 1, 10 and 50 cycles in 1.0 M KFSI in EC/DEC (1:1 vol.) electrolyte. (f-g) After 1, 10 and 50 cycles in 0.8 M KPF_6 in EC/DEC (1:1 vol.) electrolyte, respectively.

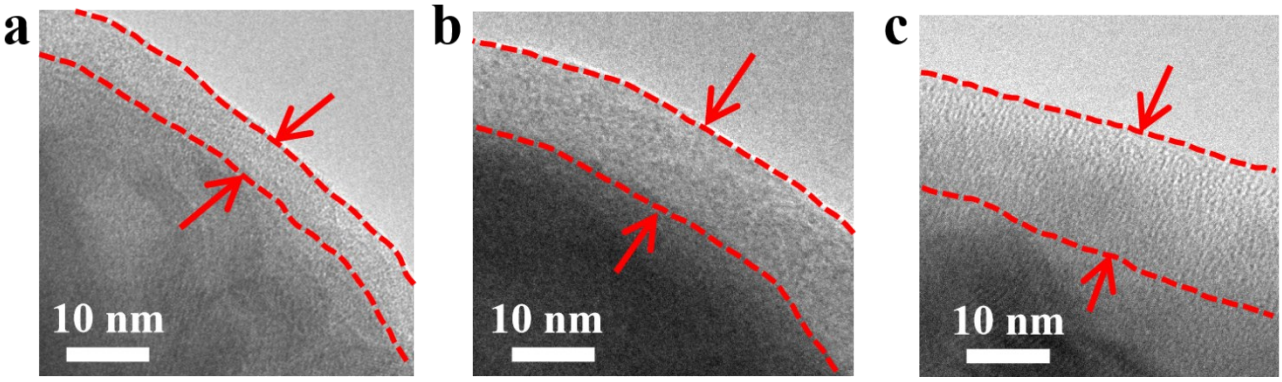

Fig. S19 TEM images of the FeP@FGCS electrodes after 50 cycles in (a) 1.0 M KFSI in DME electrolyte, (b) 1.0 M KFSI in EC/DEC (1:1 vol.) electrolyte and (c) 0.8 M KPF_6 in EC/DEC (1:1 vol.) electrolyte, respectively.

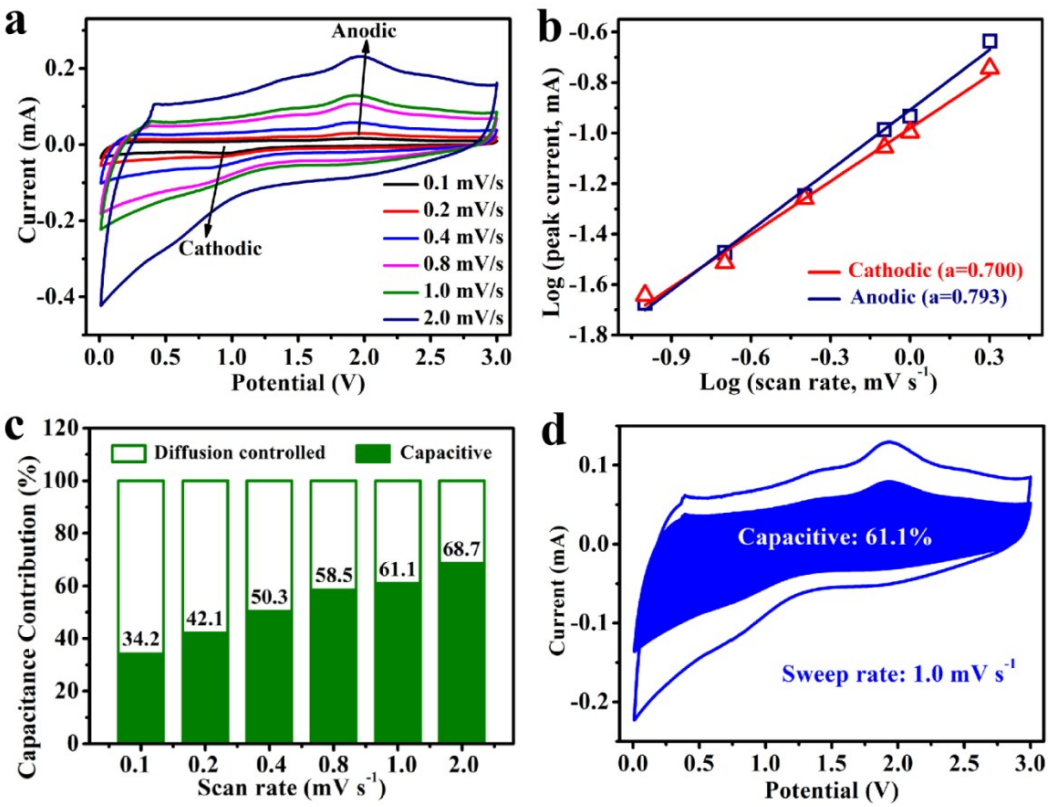

Fig. S20 (a) CV curves of the FeP@FGCS recorded at different sweep rates (0.1-2.0 mV s^{-1}) within 0.01-3.0 V (versus K^+/ K). (b) Determination of *a*-values using relationship between peak current to sweep rate. (c) Contribution ratio of pseudocapacitive and diffusion-limited effect versus sweep rates. (d) Blue curve shows CV curve of the FeP@FGCS and the shaded area indicates capacitive contribution at a sweep rate of 1.0 mV s^{-1}.

$$EC + 2e^- + 2K^+ \rightarrow K_2CO_3 + CH_2{=}CH_2 \quad (1)$$

$$2EC + 2e^- + 2K^+ \rightarrow 2ROCOOK + CH_2{=}CH_2 \quad (2)$$

$$DEC + e^- + K^+ \rightarrow C_2H_5K + OC(O\cdot)_2 \quad (3)$$

$$2ROCOOK + H_2O \rightarrow 2KHCO_3 + 2ROH + CO_2 \quad (4)$$

$$KPF_6 \rightarrow KF + PF_5 \quad (5)$$

$$PF_5 + H_2O \rightarrow POF_3 + 2HF \quad (6)$$

$$ROCOOK \text{ or } KHCO_3 + HF \rightarrow KF + ROCOOH \text{ or } H_2CO_3 \quad (7)$$

$$ROK + HF \rightarrow KF + ROH \quad (8)$$

Note S1 [1, 2] List of possible reduction and hydrolysis reactions of KPF_6 salts, ester solvents (EC and DEC) and derived components in SEI layer.

Table S1 Fitted electrochemical impedance parameters of the FeP@FGCS and pure FeP NPs electrodes before and after rate tests.

Electrodes	States	R_s (Ohm)	R_f (Ohm)	R_{ct} (Ohm)
FeP@FGCS	Before cycles	6.8	-	632.6
	After rate tests	6.1	118.7	509.3
Pure FeP NPs	Before cycles	7.6	-	1426
	After rate tests	8.2	583.5	2316

Table S2 A comparison of electrochemical potassium-ion storage properties of recently published phosphorus-based anode materials.

Anode Materials	Rate Capability	Cycling Performance	Ref.
FeP@FGCS	**221 mAh g^{-1} at 2 A g^{-1}, 164 mAh g^{-1} at 5 A g^{-1}**	**382 mAh g^{-1} after 100 cycles at 0.1 A g^{-1}, 213 mAh g^{-1} after 800 cycles at 2 A g^{-1}**	**This work**
GeP_5	343.9 mAh g^{-1} at 500 mA g^{-1}, 284.2 mAh g^{-1} at 1 A g^{-1}	213.7 mAh g^{-1} after 2000 cycles at 0.5 A g^{-1}	Ref. [3]
Sn_4P_3/C	221.9 mAh g^{-1} at 1 A g^{-1}	307.2 mAh g^{-1} after 50 cycles at 0.05 A g^{-1}	Ref. [4]
CoP⊂NPPCS	74 mAh g^{-1} at 1 A g^{-1}, 54 mAh g^{-1} at 2 A g^{-1}	114 mAh g^{-1} after 1000 cycles at 0.5A g^{-1}	Ref. [5]
P@TBMC	227 mAh g^{-1} at 1 A g^{-1}, 136 mAh g^{-1} at 2 A g^{-1}	244 mAh g^{-1} after 200 cycles at 0.5 A g^{-1}	Ref. [6]
Yolk-shell FeP@CNBs	65 mAh g^{-1} at 1 A g^{-1}, 37 mAh g^{-1} at 2 A g^{-1}	205 mAh g^{-1} after 300 cycles at 0.1 A g^{-1}	Ref. [7]
P@RGO	208.5 mAh g^{-1} at 1 A g^{-1}, 134.4 mAh g^{-1} at 2 A g^{-1}	253 mAh g^{-1} after 500 cycles at 0.5 A g^{-1}	Ref. [8]
Black Phosphorus-C	210 mAh g^{-1} at 0.2 A g^{-1}, 120 mAh g^{-1} at 0.5 A g^{-1}	270 mAh g^{-1} after 50 cycles at 0.05 A g^{-1}	Ref. [9]

Reference

1. V. Etacheri, O. Haik, Y. Goffer, G. A. Roberts, I. C. Stefan, R. Fasching and D. Aurbach, *Langmuir*, 2012, **28**, 965-976.
2. Y. Lei, L. Qin, R. Liu, K. C. Lau, Y. Wu, D. Zhai, B. Li and F. Kang, *ACS Appl. Energy Mater.*, 2018, **1**, 1828-1833.
3. W. Zhang, Z. Wu, J. Zhang, G. Liu, N.-H. Yang, R.-S. Liu, W. Pang, W. Li and Z. Guo, *Nano Energy*, 2018, **53**, 967-974.
4. W. Zhang, J. Mao, S. Li, Z. Chen and Z. Guo, *J. Am. Chem. Soc.*, 2017, **139**, 3316-3319.
5. J. Bai, B. Xi, H. Mao, Y. Lin, X. Ma, J. Feng and S. Xiong, *Adv. Mater.*, 2018, **30**, 1802310.
6. D. Liu, X. Huang, D. Qu, D. Zheng, G. Wang, J. Harris, J. Si, T. Ding, J. Chen and D. Qu, *Nano Energy*, 2018, **52**, 1-10.
7. F. Yang, H. Gao, J. Hao, S. Zhang, P. Li, Y. Liu, J. Chen and Z. Guo, *Adv. Funct. Mater.*, 2019, **29**, 1808291.
8. H. Wang, L. Wang, L. Wang, Z. Xing, X. Wu, W. Zhao, X. Qi, Z. Ju and Q. Zhuang, *Chem. - Eur. J.*, 2018, **24**, 13897-13902.
9. I. Sultana, M. M. Rahman, T. Ramireddy, Y. Chen and A. M. Glushenkov, *J. Mater. Chem. A*, 2017, **5**, 23506-23512.